PILOT
in-flight performance and first results

J.-Ph. Bernard (1), A. Mangilli (1), and the PILOT team
(1) IRAP, Toulouse France

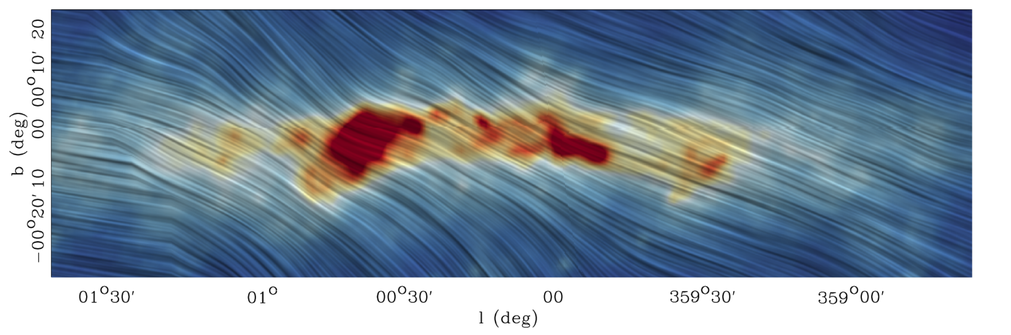

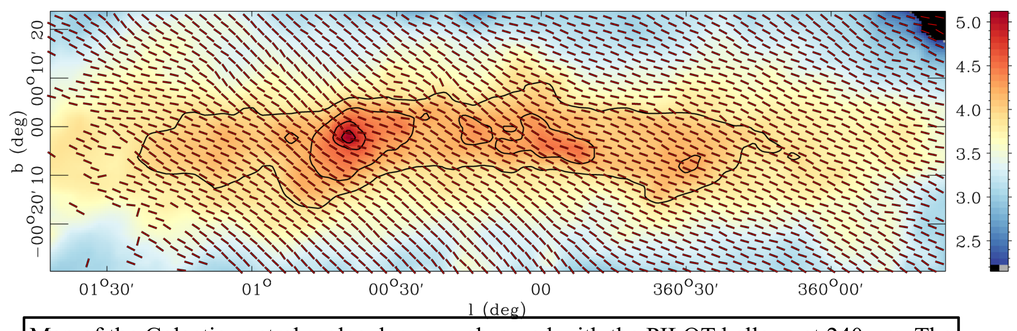

Map of the Galactic central molecular zone observed with the PILOT balloon at 240 μm. The texture, overlaid to the total intensity, shows the orientation of the magnetic field inferred from the measured dust polarization. [Mangilli et al. A&A 2019]

Summary: The Polarized Instrument for Long-wavelength Observation of the Tenuous interstellar medium (PILOT) is a balloon-borne experiment aiming at measuring the polarized emission of thermal dust at a wavelength of 240 um (1.2 THz). A first PILOT flight (flight#1) of the experiment took place from Timmins, Ontario, Canada, in September 2015 and a second flight (flight#2) took place from Alice Springs, Australia in april 2017. We present the inflight performance of the instrument during these two flights. We first present a short description of the instrument and the flights. We determine the time constants of our detectors combining in-flight information from the signal decay following high energy particle impacts (glitches) and of our internal calibration source. We use these time constants to deconvolve the data timelines and analyse the optical quality of the instrument as measured on planets. We then analyse the structure and polarization of the instrumental background. We measure the detector response flat field and its time variations using the signal from the residual atmosphere and of our internal calibration source. Finally, we analyze the detector noise spectral and temporal properties. The in-flight performances are found to be satisfactory and globally in line with expectations from ground calibrations. We conclude by assessing the expected in-flight sensitivity of the instrument in light of the above in-flight performances. The PILOT measurements n the Central Molecular Zone provide the best view of the magnetic field structure in this region and are important to understand the high star formation rate and to constrain the average galactic spectral energy distribution of polarized light up to the Far-Infrared.This posters summarizes findings described in [Mangilli et al. Exp. Astronomy 2019] and [Mangilli et al. A&A 2019].

PILOT:

A description of the instrument is available in Bernard et al 2016. Table 1 summarizes the main characteristics. The optics is composed of an off-axis paraboloid primary mirror (M1) of 0.83m diameter and an off-axis ellipsoid secondary mirror (M2). All optics following M1 is cooled at cryogenic temperature of 2 K. The telescope is followed by a re-imager and a polarimeter through a flat mirror (M3). Two lenses (L1 and L2) are used to re-image the focus of the telescope onto the detectors. A Lyot-stop is placed between the lenses at a pupil plane that is conjugate of the primary mirror. A rotating Sapphire Half-Wave Plate (HWP), is located next to the Lyot-stop, which introduces a phase delay between the two orthogonal components of the incident light. A polarization analyzer is placed at a 45° angle in front of the detectors, in order to transmit one polarisation to the transmission (TRANS) focal plane and reflect the other polarisation to the reflection (REFLEX) focal plane. Observations at, at least two, different HWP angles allow us to reconstruct the stokes parameters I, Q and U. Each of the TRANS and REFLEX focal planes include 2048 bolometers (8 arrays of 16 X 16 pixels)cooled to 300 mK by a closed cycle He3 fridge. The pointing uses data from the Estadius stellar sensor (Montel+2015), which provides an angular resolution of a few arc seconds for scanning at speeds up to a 1°/s. An internal calibration source (ICS) is used to calibrate time variations of the detector responses.

Flight#1 of the PILOT experiment took place from the launch-base facility at the airport of Timmins, Ontario, Canada on September 21, 2015.
Flight#2 was conducted from the USA-operated launch base of Alice Springs, Australia on April 16 2017. The launches were part of campaigns led by CNES and the local Space Agencies (CSA, NASA). In both cases the gondola was recovered safely at the end of the flight.

Telescope Type	Gregorian	
Equivalent focal length [mm]	1790	
Numerical aperture	$F/2.5$	
FOV [°]	1.0×0.8	
Ceiling altitude	~3 hPa	
Pointing reconstruction	translation= 1″, rotation= 6″, 1σ	
Gondola Mass	~1100 kg	
Primary mirror type	Off-axis parabolic	
Primary mirror dimension [mm]	930 x 830	
M1 used surface projeted diameter [mm]	730	
Focal length [mm]	750	
Detector type	Multiplexed bolometer arrays	
Number of Detectors	2048	
Detector temperature [mK]	300	
Sampling rate [Hz]	40	
Photometric channels	SW Band	LW Band
λ_0 [μm]	240	550
ν_0 [GHz]	1250	545
$\Delta\nu/\nu$	0.27	0.31
beam FWHM [′]	1.9	3.3
Minimum Strehl Ratio	0.95	0.98

Tab 1: Main characteristics of the PILOT instrument.

Optics:

During each flight, we observed planets which are point sources at the resolution of PILOT and can be used to assess the optical quality through a measurement of the instrument Point Spread Function (PSF). Planet maps were constructed with a pixel size of 0.1' for each detector array. Data were corrected for the responses calculated on the atmospheric signal and for the effects of the time constant of the detectors.
The parameters of the PSF were deduced using an elliptical Gaussian fit applied to the images.
Fig. 2 shows the values obtained for the major and minor axis dimensions of the PSF obtained on Jupiter. We obtain an average full-width half maximum (FWHM) size of 2.25'+-0.15', taking into account the apparent size of the planet. The boxy shape of the PSF is explained by the convolution with the pixel size, as shown from the comparison with a simulation. The wings of the PSF are probably due to diffraction, which is not included in the simulation.

Detector time constants:

We fit the progressive signal decay following illumination by the ICS in order to derive the detector optical time constants. However, this decay time has a contribution due to the ICS itself, which we estimate by comparison with the time constant values derived from fitting the signal decay after glitches, which are produced by the interaction with high energy particles. We used glitches above 100 ADU (rate=2.24 gli/pix/hr). We derived a time constant for the ICS of 10.2 ms (0.4 samples). The average detector optical time constant is 17.5 ms (0.7 samples)The map of the detector time constants derived are shown in Fig. 1.

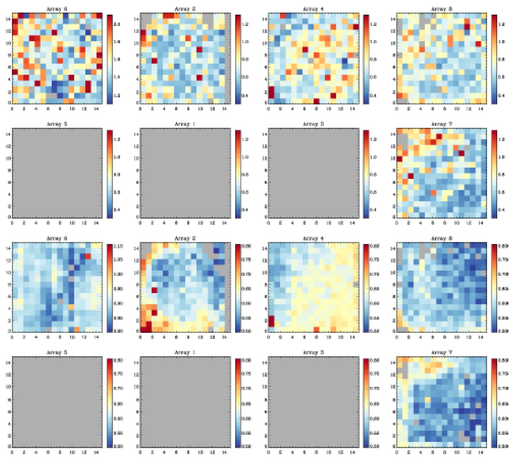

Fig 1: Top: Focal plane distribution of the bolometer time constants as measured from glitches. Bottom: Focal plane distribution of the bolometers time constants as measured using the ICS downward transitions. The four arrays shown on the left (resp. right) belong to the TRANS (resp. REFLEX) focal plane.

Response calibration:

We measure the spatial distribution of the detector response using the residual atmospheric emission. We measure the slope of the correlation between the bolometer signal and the pointing elevation during science observations obtained at variable elevation angle. Fig. 3 shows the focal plane map of the mean response. The pattern is also similar to that observed during ground test where the focal planes were operated in front of an extended black-body. The accuracy of the response map is at the 1 % level or better when using all observations. This confirms the advantage of using a scanning strategy with varying elevation as implemented for flight #2.

We measure the time variations of the detector response using the ICS signal. Fig 4 shows the time variations of the array-averaged detector response to the ICS signal for array#6 during flight #2. The variations in the response with time are about 10 % for all arrays. Step-like variations are clearly seen in both the TRANS and REFLEX arrays. These variations are mostly caused by variations of the background level on the detectors. Some are due to changes of the observation elevation, which changes the intensity of the residual atmospheric emission. Some are caused by observing with different HWP angles, which, due to the polarization of the instrumental background (see Misawa et al. 2017), changes the detector background.

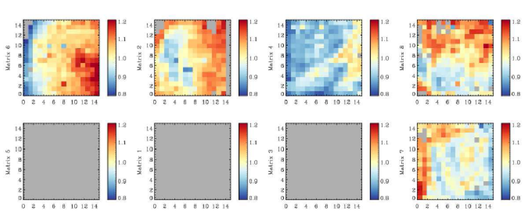

Fig 3:Focal plane map of the mean response computed on the residual atmospheric signal during all scientific observations of flight #2. The response map has been divided by its average over valid detectors so that it has a mean equal to unity.

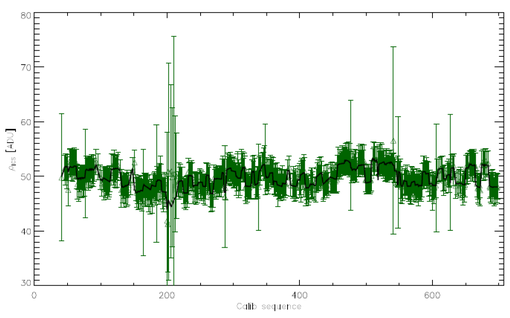

Fig 4: Array-averaged ICS response for array #6 as a function of the calibration sequence number (green) compared to the predictions of a simple best fit parametric model (black) based on background intensity and observation elevation.

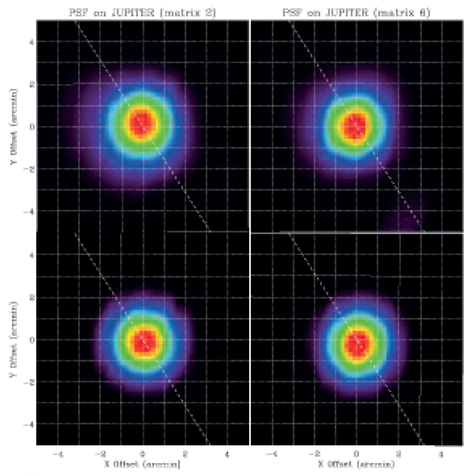

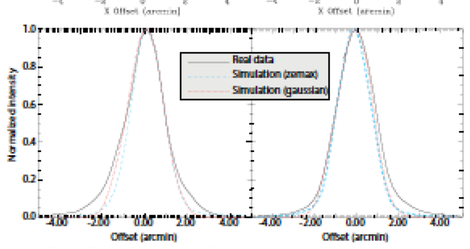

Fig 2:Top: Images of Jupiter obtained with array #2 (left) and 6 (right) during one of the observing sequence of the planet. Middle: Map obtained on array #2 (left) and #6 (right) from signal simulated using the actual pointing (see text). The scan direction is shown by the dashed white line. Bottom: Circular average profile of the PSF measured on array #2 (left) and array #6 (right). The solid black curve corresponds to measurements from the observations on Jupiter during flight #2. The dashed curves show predictions from simulations using optics prediction and convolution with pixel extent.

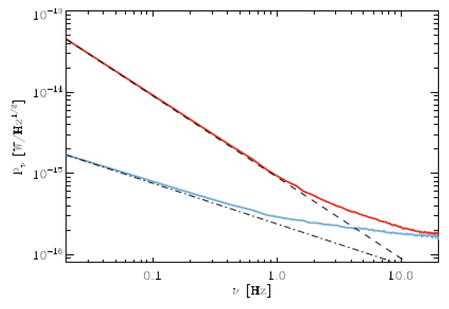

Fig 5: Array #6 array-flight-averaged noise power spectrum (red) and HPD flight-average (blue) in W/√Hz, during flight #2. 1/ν and 1/√ν curves are over plotted to guide the eye as dashed- and dashed-dotted-lines, respectively.

Noise properties :

The calibrated timelines are corrected for the atmospheric signal to first order, by removing their linear correlation with observation elevation. The array-averaged power spectra are computed for each detector array and each scan. We take the median value among the scans as the flight-averaged noise power spectra.
Similarly, we split each detector array in two subsets with the same number of pixels, chosen randomly, and compute the half-difference of the two detector-averaged timelines. From these half-pixel difference (HPD) timelines, we compute the HPD power spectra, which do not contain the common mode.

The flight-averaged noise power spectra are shown in Fig. 5 for array #6. The spectra are qualitatively similar for other detector arrays. At high frequency, a flat spectrum component is observed, corresponding to white noise, presumably caused by photon noise. At low frequency rise with NEP α 1/ν and 1/√ν components are observed for noise and HDP, respectively. The former contains residuals from atmospheric emission and possibly variations of the focal plane temperature that contribute to the low-frequency rise. In the HPD case, we can consider that all atmospheric and temperature variations are removed with the per-array common mode.

The focal plane median high-frequency noise noise equivalent power observed during flight#2 is 4.6 10^{-16} W/√Hz. Array #6 is the most sensitive, with a median NEP of 1.9 10^{-16} W/√Hz. Other arrays have NEPs ranging from 4.5 to 6 10^{-16} W/√Hz.

Figure 6 shows the array-averaged time-frequency plots for both signal and HPD during flight #2. Some observations can be identified, having a larger low-frequency component, due to actual signal and/or the simple atmospheric emission removal we have implemented here, that sometimes fails to properly subtract the low-frequency contribution. At higher frequency, a good stability of the white noise is observed outside these observations. In the HPD case, where the common mode for all the detectors belonging to the same array has been removed, the stability is remarkable for both low and high frequencies, during the whole duration of the observations.

Fig 6: Time-frequency behaviour of the total array-averaged power spectra (top) and of the half-pixel difference power spectra (HPD, bottom) for array #6 during flight #2, in units of log10(W/√Hz). Individual noise power spectra are computed for the array-average total signal or half-pixel differenced signal, for each individual observing scan.

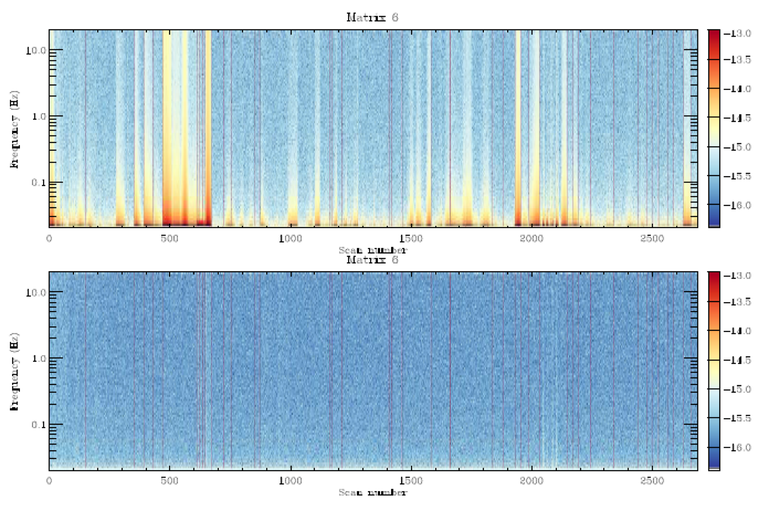

First results on the Galactic center

From our measured dust polarization angles, we infer a magnetic field orientation projected onto the plane of the sky (POS) that is remarkably ordered over the full extent of the Central Molecular Zone (CMZ), with an average tilt angle of ≃ 22° clockwise with respect to the Galactic plane. Our results confirm previous claims that the field traced by dust polarized emission is oriented nearly orthogonally to the field traced by GHz radio synchrotron emission in the Galactic Center region. The observed field structure is globally compatible with the latest *Planck* polarization data at 353 GHz and 217 GHz. Upon subtraction of the extended emission in our data, the mean field orientation that we obtain shows good agreement with the mean field orientation measured at higher angular resolution by the JCMT within the 20 km/s and 50 km/s molecular clouds. We find no evidence that the magnetic field orientation is related to the 100 pc twisted ring structure within the CMZ. The low polarization fraction in the Galactic Center region measured with *Planck* at 353 GHz combined with a highly ordered projected field orientation is unusual. This feature actually extends to the whole inner Galactic plane. We propose that it could be caused by the increased number of turbulent cells for the long lines of sight towards the inner Galactic plane or to dust properties specific to the inner regions of the Galaxy. Assuming equipartition between magnetic pressure and ram pressure, we obtain magnetic field strength estimates of the order of 1 mG for several CMZ molecular clouds.

References :
- A. Mangilli and the PILOT team, Experimental Astronomy 2019, in press, arXiv180405645F
- A. Mangilli and the PILOT team, A&A 2019 in press
- J.P. Bernard, the PILOT team, Experimental Astronomy **42**, 199 (2016).
- C. Engel, I. Ristorcelli, J.P. Bernard, Y. Longval, C.Marty, B.Mot, G. Otrio, G. Roudil, Experimental Astronomy **36**, 21 (2013).
- J. Montel, Y. Andre, F. Mirc, P. Etcheto, J. Evrard, N. Bray, M. Saccoccio, L. Tomasini, E. Perot, in *22nd ESA Symposium on European Rocket and Balloon Programmes and Related Research*, *ESA Special Publication, vol. 730, ed. by L. Ouwehand (2015), ESA Special Publication*, vol. 730, p. 509
- R. Misawa, the PILOT team, Experimental Astronomy **43**, 211 (2017).